Evolution of constitution, structure, and mechanical properties in Fe–Ti–Zr–B heterogeneous multiphase composites

Jin Man Park
Leibniz Institute for Solid State and Materials Research Dresden, Institute for Complex Materials, D-01171 Dresden, Germany; and Center for Non-Crystalline Materials, Department of Metallurgical Engineering, Yonsei University, Seoul 120-749, Republic of Korea

Do Hyang Kim[a)]
Center for Non-Crystalline Materials, Department of Metallurgical Engineering, Yonsei University, Seoul 120-749, Republic of Korea

Ki Buem Kim
Department of Advanced Materials Engineering, Sejong University, Seoul 143-747, Republic of Korea

Norbert Mattern
Leibniz Institute for Solid State and Materials Research Dresden, Institute for Complex Materials, D-01171 Dresden, Germany

Jürgen Eckert[b)]
Leibniz Institute for Solid State and Materials Research Dresden, Institute for Complex Materials, D-01171 Dresden, Germany; and TU Dresden, Institute of Materials Science, D-01062 Dresden, Germany

(Received 23 June 2010; accepted 21 September 2010)

The constituent phases, the microstructure, and the mechanical properties of a series of $Fe_{87-x}Ti_7Zr_6B_x$ (x = 0, 2, 4, 6, 8, 10, and 12) alloys produced by copper mold casting were investigated. Partial substitution of iron by boron in the $Fe_{87}Ti_7Zr_6$ ultrafine eutectic alloy induces phase/microstructural evolution and simultaneously changes the mechanical properties. In the composition range of $2 \leq x \leq 6$, the typical lamellar structure slightly changes into a spherical cellular-type eutectic. For $8 \leq x \leq 12$, multiphase composites containing a glassy phase form. The ultrafine eutectic composites exhibit a high compressive strength of ~2.9–3.1 GPa and a distinct plasticity of ~2–8%, whereas the glassy matrix composites show a high strength of ~3.1–3.3 GPa but no observable macroscopic plasticity before failure. These findings reveal that the plasticity of heterogeneous multiphase composites is strongly related to the length scale variables and the crystallinity of the constituent phases.

I. INTRODUCTION

Rapid solidification has been well known to produce nonequilibrium microstructures and allows for structural refinement, the formation of novel crystalline or amorphous phases, and extension of solid solubility.[1] Thus, research on amorphous and nanostructured materials continue to receive great attention, because they show many unique mechanical, physical, and chemical properties in comparison to the corresponding coarse-grained crystalline alloys.[2,3] However, these materials deformed mainly by highly localized shear bands, and thus exhibit very limited macroscopic room temperature plasticity before fracture.[2,3] To overcome this limitation, hybrid composites coexisting of a soft phase in combination with a hard amorphous or complex nano-/ultrafine crystalline matrix have been developed for a variety of alloy systems.[4–11] Among them, Fe-based alloys are most attractive for engineering applications, because they possess high strength, good soft magnetic properties, and high corrosion resistance in some cases.[12] Moreover, Fe-based alloys are rather inexpensive due to the abundance of natural resources and low material cost.

Following this approach, Fe-based bulk metallic glass (BMG) matrix composites containing in situ formed micrometer-sized precipitates or dendrites have been developed by Shen et al.[13] and Guo et al.[14] The former composites were obtained by addition of Cu, which is virtually insoluble in Fe at room temperature into an Fe–Co–B–Si–Nb alloy, while the latter were achieved by systematic composition fine-tuning of an Fe–Mo–P–C–B alloy. On the other hand, nano-/ultrafine structured composites were reported for multicomponent Fe–Cr–Mo–Ga–C and Fe–Co–Mo–C–B–Si alloys derived from an BMG-forming composition[15,16] and developed in simple

[a)]Address all correspondence to this author.
e-mail: dohkim@yonsei.ac.kr
[b)]This author was an editor of this journal during the review and decision stage. For the *JMR* policy on review and publication of manuscripts authored by editors, please refer to http://www.mrs.org/jmr_policy
DOI: 10.1557/jmr.2010.50

 © Materials Research Society 2011

https://doi.org/10.1557/jmr.2010.50 Published online by Cambridge University Press

binary Fe–Zr and pseudobinary (Fe, Al)–Nb eutectic alloys on the basis of the equilibrium phase diagram.[17,18] These different kinds of novel heterogeneous composites show clearly improved room temperature plastic deformability and high strength.[15–18] The enhanced plasticity possibly stems from the formation of multiple shear bands initiated at the interface between the micrometer-sized ductile phases and the metallic glass/nanocrystalline matrix, and their confinement between the micrometer-sized ductile phases in the matrix.[19–26]

In this study, we chose the simple pseudobinary $Fe_{87}Ti_7Zr_6$ alloy with ultrafine regular lamellar eutectic structure as the starting composition[27] and explored the effect of boron addition on the microstructure evolution and the resulting mechanical properties. It is well known that there are strong atomic interactions, large differences in atomic size, and a large negative enthalpy of mixing between boron and transition metals.[12] This may not only significantly decrease the melting temperature and the diffusivity of the liquid/amorphous alloy at suitable atomic ratios of boron to transition metals, resulting in an improvement of its glass-forming ability and thermal stability, but also influences the phase and microstructure development and the mechanical properties. As mentioned previously, the mechanical properties of heterogeneous composites, especially with regard to plasticity, strongly depend on the microstructural features including phase constitution and the length scale of the constituent phases. Here, we report on the phase formation, microstructure and resulting mechanical properties of as-cast $Fe_{87-x}Ti_7Zr_6B_x$ (x = 0, 2, 4, 6, 8, 10, and 12) heterogeneous multiphase composites. We found that a high strength of ~3.1 GPa and an enhanced compressive plastic strain of ~8% can be achieved for the $Fe_{83}Ti_7Zr_6B_4$ ultrafine eutectic composite, caused by the design of a novel microstructure with ultrafine scale and spatial length-scale heterogeneity.

II. EXPERIMENTAL

Alloy ingots (20 g) with nominal compositions of $Fe_{87-x}Ti_7Zr_6B_x$ (x = 0, 2, 4, 6, 8, 10, and 12) were prepared by arc melting of high purity elements (99.99 wt%) under an argon atmosphere followed by direct casting into cylindrical rods with 1 mm diameter and 30 mm length using a suction casting facility. Thermal properties were measured using differential scanning calorimetery (DSC; Perkin Elmer DSC7, Boston, MA) and differential thermal analysis (DTA; Perkin Elmer DTA7) at a constant heating rate of 0.16 K/s under a flow of purified argon. X-ray diffraction (XRD; Rigaku CN2301, monochromatic Cu K_α radiation, Tokyo, Japan) experiments were used for structural characterization. The microstructure of the cast samples was analyzed by scanning electron microscopy (SEM; JEOL JSM-6390, Tokyo, Japan). To evaluate the mechanical properties under compression, cylindrical specimens with a 2:1 aspect ratio were prepared and tested under quasi-static loading at an initial strain rate of 1×10^{-4} s^{-1} at room temperature. The lateral and fracture surface morphologies of failed samples were investigated by SEM.

III. RESULTS AND DISCUSSION

Figure 1 shows XRD patterns of the as-cast $Fe_{87-x}Ti_7Zr_6B_x$ (x = 0, 2, 4, 6, 8, 10, and 12) alloys. For x = 0 ~6, only two crystalline phases can be identified in the rapidly solidified alloys. One is the α-Fe solid solution phase; the other one is the Fe_2Ti Laves phase. The lattice parameters of both phases (α-Fe: a = 0.2872 nm and Fe_2Ti: a = 0.484 nm, c = 0.792 nm) are larger than those of pure α-Fe (a = 0.28664 nm) and equiatomic Fe_2Ti (a = 0.4785 nm and c = 0.7799 nm), most likely due to dissolution of Ti and Zr in α-Fe and of Zr in the Fe_2Ti Laves phase.[28–30] On the other hand, in the composition range of 8 to ~12, the XRD patterns show several crystalline peaks superimposed on a broad diffuse diffraction background, indicating the formation of a mixture of crystalline and amorphous phases. The diffraction peaks of the crystalline phases were analyzed as the body-centered-cubic (bcc) structure of an α-Fe solid solution (a = 0.287 nm) and the body-centered-tetragonal structure of the Fe_2B phase with lattice parameters a = 0.511 nm and c = 0.4249.[28] According to the amount of boron addition, the XRD patterns indicate that one of the competing crystalline phases changes from Fe_2(Ti, Zr) to

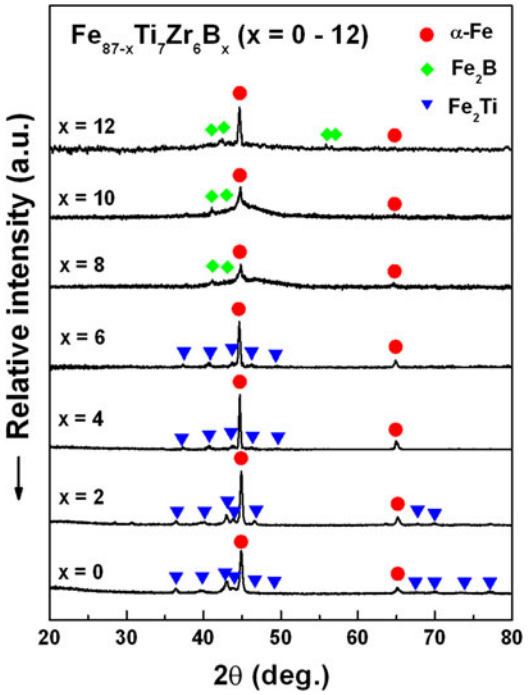


FIG. 1. XRD patterns of the as-cast $Fe_{87-x}Ti_7Zr_6B_x$ (x = 0–12) alloys.

https://doi.org/10.1557/jmr.2010.50 Published online by Cambridge University Press

Fe_2B phase regardless of the α-Fe solid solution phase, which is also corroborated by TEM investigations (not shown here).[27] This reveals that the crystallinity and phase constitution of the Fe–Ti–Zr–B ultrafine composites strongly depend on the boron content.

Figure 2 shows DTA and DSC traces of the as-cast $Fe_{87-x}Ti_7Zr_6B_x$ (x = 0, 2, 4, 6, 8, 10 and 12) alloys during continuous heating at a rate of 0.16 K/s. For all samples, the DTA curves show two endothermic peaks during the melting process. One is near liquidus; the other is near solidus. The melting temperatures (T_m) and liquidus temperatures (T_l) are marked by arrows in the DTA traces and are summarized in Table I. With addition of 2 at.% boron, T_l and T_m decrease abruptly from 1601 to 1565 K and from 1551 to 1461 K, respectively. In the composition range of $2 \le x \le 6$, T_l steadily decreases, while T_m maintains an almost constant temperature, which indicates that these three alloys are at the same hypoeutectic region. In contrast, as x increases further ($8 \le x \le 12$), T_l increases gradually, whereas T_m maintains almost the same temperature, which can be attributed to the existence of another hypoeutectic region. Combined with the information of the constituent phases for each alloy (see Fig. 1), we can regard $Fe_{87-x}Ti_7Zr_6B_x$ (x = 0, 2, 4, 6, 8, 10, and 12) alloys as a simple Fe–Fe_2(Ti, Zr) and a Fe–Fe_2B pseudobinary system in the composition range of $2 \le x \le 6$ and $8 \le x \le 12$, respectively. These results match well with the phase analysis results (see Fig. 1). As shown in the inset in Fig. 2, when the boron concentration (x) is in the range between 8 and 12, all DSC traces exhibit one endothermic event characteristic of the glass transition from an amorphous solid into a supercooled liquid, followed by an exothermic crystallization reaction, which is characteristic for an amorphous phase. The onset of the glass transition (T_g) and the onset temperature of crystallization (T_x) are marked by arrows and the exothermic heat flow (ΔH) of the first crystallization step is given in DSC traces. The thermal properties of all investigated alloys are listed in Table I. For x = 8 and 10, T_g exhibits nearly the same temperature of 830 K but ΔH is slightly different −11.8 and −14.3 J/g, respectively. As the B content further increases (x = 12), T_g and T_x shift to higher temperatures and ΔH (= −5.2 J/g) strongly decreases. These results reveal the formation of an amorphous phase as a constituent phase during solidification within the composition range of $8 \le x \le 12$. The volume fraction of the amorphous phase, as obtained from DSC analysis by comparing the heat of crystallization released in the DSC scans for the composites relative to that of a fully glassy ribbon (not shown here), is estimated to be around 16, 20, and 7 vol% for x = 8, x = 10, and x = 12, respectively.

Figure 3 shows SEM secondary electron micrographs obtained from the as-cast $Fe_{87-x}Ti_7Zr_6B_x$ (x = 0, 2, 4, 6, 10, and 12) alloys. Figure 3(a) displays a typical regular lamellar eutectic microstructure consisting of alternating dark and bright contrast phases. The average lamellar spacing is 200–300 nm. When a small amount of boron is added ($2 \le x \le 6$), the eutectic structures are drastically modified from a regular lamellar-type eutectic to an irregular cellular-type eutectic. As shown in Figs. 3(b)–3(d), the cellular-type eutectics exhibit length-scale heterogeneity of the lamellar spacing, i.e., ultrafine scale eutectic areas (core) are surrounded by large-scale eutectic areas

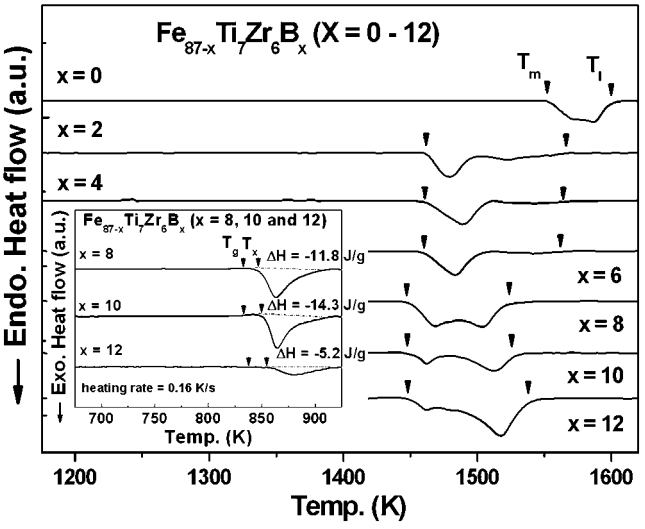


FIG. 2. DTA traces (heating rate 0.16 K/s) of the as-cast $Fe_{87-x}Ti_7Zr_6B_x$ (x = 0–12) alloys. The inset shows DSC traces (heating rate 0.16 K/s) of the as-cast $Fe_{87-x}Ti_7Zr_6B_x$ alloys with x = 8, 10, and 12.

TABLE I. Thermal and mechanical properties of the as-cast $Fe_{87-x}Ti_7Zr_6B_x$ (x = 0–12) alloys with 1 mm diameter.

Composition (at.%)	T_g (K)	T_{x1} (K)	$\lvert\Delta H_1\rvert$ (KJ/mol)	T_m (K)	T_l (K)	σ_y (MPa)	ϵ_y (%)	σ_{max} (MPa)	ϵ_p (%)
$Fe_{87}Ti_7Zr_6$	...	...	...	1551 ± 1	1601 ± 1	2600 ± 30	1.8 ± 0.1	2700 ± 75	0.5 ± 0.2
$Fe_{85}Ti_7Zr_6B_2$	...	...	...	1461 ± 1	1565 ± 1	2800 ± 25	1.8 ± 0.1	2942 ± 60	2 ± 1
$Fe_{83}Ti_7Zr_6B_4$	...	...	...	1461 ± 1	1556 ± 1	2743 ± 20	1.8 ± 0.1	3075 ± 45	8 ± 2
$Fe_{81}Ti_7Zr_6B_6$	...	...	...	1459 ± 1	1555 ± 1	2945 ± 20	1.8 ± 0.1	3100 ± 50	2 ± 1
$Fe_{79}Ti_7Zr_6B_8$	830 ± 1	850 ± 1	11.8 ± 1.2	1448 ± 1	1524 ± 1	3233 ± 30	1.9 ± 0.1	3233 ± 75	...
$Fe_{77}Ti_7Zr_6B_{10}$	830 ± 1	853 ± 1	14.3 ± 1.5	1448 ± 1	1524 ± 1	3265 ± 35	1.9 ± 0.1	3265 ± 80	...
$Fe_{75}Ti_7Zr_6B_{12}$	835 ± 1	857 ± 1	5.2 ± 0.7	1448 ± 1	1536 ± 1	3298 ± 30	1.9 ± 0.1	3298 ± 70	...

T_g, onset temperature of the glass transition; T_x, crystallization temperature; ΔH, exothermic heat of crystallization; T_m, melting temperature; T_l, liquidus temperature; σ_y (0.2% offset), yield stress; H_v, Vickers hardness; ϵ_y, yield strain; σ_{max}, ultimate compressive stress; ϵ_p, plastic strain.

https://doi.org/10.1557/jmr.2010.50 Published online by Cambridge University Press

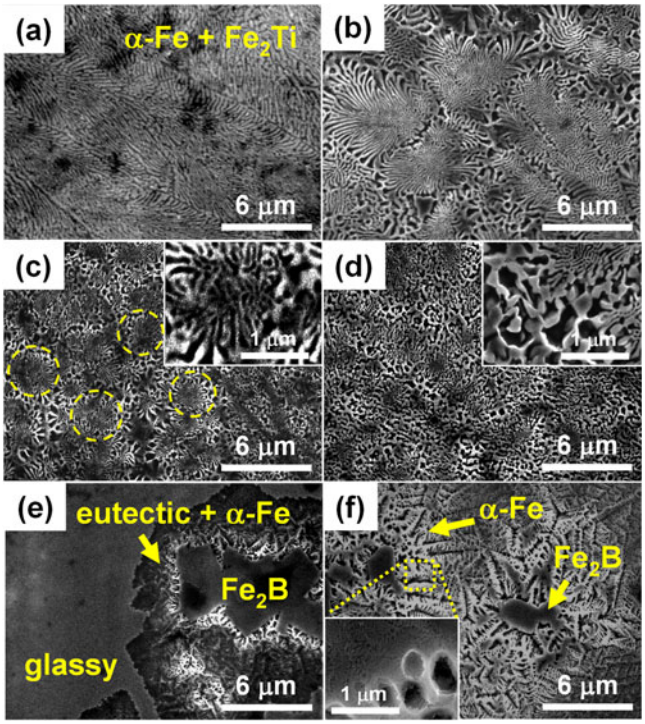


FIG. 3. Secondary electron SEM images of the as-cast $Fe_{87-x}Ti_7Zr_6B_x$ (x = 0–12) alloys; (a) x = 0, (b) x = 2, (c) x = 4, (d) x = 6, (e) x = 10, and (f) x = 12.

(boundary). The average lamellar spacings of the core and boundary regions are ~100 and ~800 nm (x = 2), ~100 and ~500 nm (x = 4), and ~100 and ~700 nm (x = 6), respectively. In particular, in the case of x = 4, the eutectic cells are finer (2–4 μm) and have a more pronounced spherical shape compared to the x = 2 and 6 alloys. EDX analysis reveals that the dark contrast phases are enriched in Fe (98.9 ± 0.8 at.%), while the bright contrast layers are enriched in Ti (9 ± 1 at.%) and Zr (9.5 ± 1 at.%) compared to nominal alloy composition. On the basis of the XRD and EDX analysis results, the alternating phases are identified as bcc α-Fe solid solution and hexagonal-close-packed Fe_2Ti.

With further increasing of the amount of boron (up to x = 12), the phase constitution and microstructure evidently change from an ultrafine alternating two-phase structure to a multiphase complex structure containing a glassy phase (see Fig. 1 and inset of Fig. 2). The overall macroscopic microstructures of multiphase composites present similar characteristics ($8 \leq x \leq 12$). Only the thickness of the glassy layer in the edge of rod samples, i.e., volume fraction of the glassy phase, change with an increase of boron content (not shown here). As shown in Figs. 3(e) and 3(f), the complex structure exhibits a hierarchical length-scale gradient in the constituent phases including glassy, ultrafine eutectic, submicron-scale dendrite, and micron-scale intermetallic phases. The Fe_2B phase heterogeneously nucleates first, followed by dendritic-type solidification of the remaining liquid into Fe-enriched zones surrounding the solute-rich intermetallic Fe_2B phase. As shown by the enlarged view of the dashed squared region [inset in Fig. 3(f)], the α-Fe dendrites nucleate and grow, together with a nanoscale eutectic in the interdendritic regions. The melt freezes into a glassy state at the contact surface of the mold where the cooling rate is highest, while in the inner parts of the samples experiencing a lower cooling rate the melt solidifies by nucleation and growth of crystals due to the cooling rate gradient. The aforementioned phase and microstructural investigations allow classifying these composites into two different groups. The first group of composites is characterized by an ultrafine alternating two-phase eutectic consisting of α-Fe and Fe_2(Ti, Zr) phases. The second group comprises multiphase composites composed of glassy, ultrafine scale eutectic and dendrites, and micrometer-size intermetallic phases. Thus, it is evident that the boron content is decisive for the microstructural evolution of Fe–(Ti, Zr) pseudobinary eutectic alloys.

The room temperature mechanical properties of the as-cast $Fe_{87-x}Ti_7Zr_6B_x$ (x = 0, 2, 4, 6, 8, 10, and 12) alloys were checked by room temperature compression tests. Figure 4 shows room temperature engineering compressive stress–strain curves for all investigated alloys and the obtained mechanical properties are summarized in Table I. To assure the reliability of the mechanical property data, the values given in Table I were determined from the average values of a minimum of five measurements for each sample. The compressive plasticity clearly depends on the type of composite. The ultrafine eutectic composites (x = 2–6) show a high strength of 2.9–3.1 GPa and a distinct plasticity of 2–8%, whereas the multiphase composites (x = 8–12) exhibit a high strength of 3.1–3.2 GPa but no appreciable plastic strain. These findings reveal that the crystallinity of the constituent phases, the length scale and the distribution of the crystalline phases play a decisive role on the mechanical properties.

To investigate the deformation behavior of the two different types of heterogeneous ultrafine composites in more detail, the fractured samples with x = 4 and x = 10 were selected and carefully examined by SEM. Figure 5 displays secondary electron SEM images of the outer appearance of the samples, and the fracture and lateral surface morphologies of the fractured specimens. Figure 5(a) clearly shows that the fracture of the ultrafine eutectic alloy (x = 4; $Fe_{83}Ti_7Zr_6B_4$) occurs along the maximum shear plane, which is inclined by about 45° to the direction of the applied load. Figure 5(c) shows an enlarged view of marked region (i) in Fig. 5(a), exhibiting numerous shear bands on the side view of the deformed sample. The shear bands are wavy and their propagation is discontinuous, unlike the typical shear bands in BMGs and nanocrystalline alloys. This reveals that there is no significant shear localization during deformation. In addition, the fracture

https://doi.org/10.1557/jmr.2010.50 Published online by Cambridge University Press

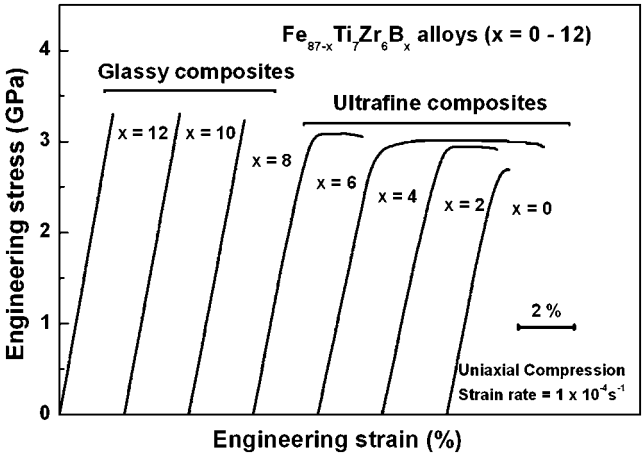


FIG. 4. Compressive stress–strain curves of the as-cast $Fe_{87-x}Ti_7Zr_6B_x$ (x = 0–12) alloys.

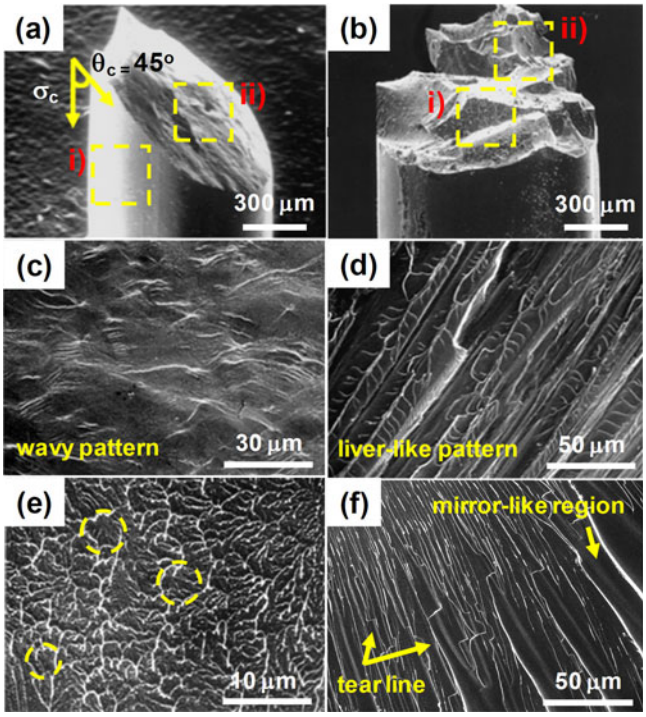


FIG. 5. Secondary electron SEM images taken from the failed samples of as-cast $Fe_{87-x}Ti_7Zr_6B_x$ (x = 4 and 10) alloys: outer appearances (a) x = 4, (b) x = 10; lateral surfaces (c) x = 4; fracture surfaces (e) x = 4, (d, f) x = 10, respectively.

surface morphology [Fig. 5(e)] displays dimplelike characteristics indicating ductile fracture behavior, as marked by region (ii) in Fig. 5(a).[31] Interestingly, the size of the dimplelike areas matches that of the spherical eutectic colonies well [see Fig. 3(c)]. This suggests that the distinct length-scale heterogeneity of the lamellar spacing and the eutectic cell size and the shape of the colonies are important for controlling the plastic deformability. As previously reported for an ultrafine eutectic Ti–Fe–Sn alloy,[32] it is feasible to suppose that these unique microstructures of the heterogeneous ultrafine composites counteract the otherwise often observable plastic deformation and failure instability. Apparently, these microstructures allow for efficient dissipation of the shear stress and accommodation of excessive shear strain occurs during deformation, caused by a rotation of the coarse eutectic areas against the fine eutectic areas acting as a pivoting point. The rotational motion of spherical colonies with bimodal length scale can effectively accommodate complex plastic flow states without preferential direction, and promotes the macroscopic compressive plasticity. As a result, the plasticity of ultrafine eutectic composites is not only related to the length-scale heterogeneity of the eutectic phases but is also associated with deformation-induced rotation of eutectic colonies.

On the other hand, in the case of the glassy composite (x = 10; $Fe_{77}Ti_7Zr_6B_{10}$), the samples break into a large number of pieces and the fracture surface shown in Fig. 5 (b) displays a relatively irregular feature. Figures 5(d) and 5(f) show enlarged views of the fracture surface morphologies for the regions marked regions (i) and (ii) in Fig. 5 (b), respectively. Region (i) displays a liverlike pattern suggesting that local viscous flow correlated with strain softening occurs, as is often observed for high strength BMGs.[3] Meanwhile, region (ii) exhibits cleavage features composed of mirrorlike regions and tear lines, indicating that fracture occurs in a brittle manner when the local shear stress is exceeded.[31] This anomalous mixed fracture morphology can be ascribed to the inhomogeneous microstructure, i.e., the local cooling rate-dependent microstructural gradient observed along the cross section of the as-cast cylinders [Fig. 3(e)]. Regarding these investigations, the structural heterogeneity including glassy and composite crystalline phases and, in particular, the thickness of the glassy layer and the interface stability between the glassy and crystalline phases play a critical role on the overall mechanical performance, especially on the plasticity for the samples with boron content above 6%. Accordingly, it is reasonable that the fracture of the $Fe_{77}Ti_7Zr_6B_{10}$ alloy with structural inhomogeneity between the center and the edge of the as-cast rod samples takes place catastrophically without macroscopic plastic strain resulting from the fracture and deformation instability.

In general, for application of advanced structural materials, the understanding of the structure-property correlation is very important. In this study, a distinct microstructural evolution and enhanced mechanical properties can be observed by just partially replacing iron by boron in the Fe–(Ti, Zr) ultrafine eutectic alloy. Obviously, the spatial heterogeneity in terms of the morphology and the size of the eutectic is a potential reason to generate the different plasticity and work hardenability

https://doi.org/10.1557/jmr.2010.50 Published online by Cambridge University Press

for homogeneous ultrafine eutectic composites, as shown in Figs. 3, 4, and 5.[32–34] This may degrade the local elastic stiffness and assist a wavy propagation of shear bands. Furthermore, the fracture characteristics obtained from deformed samples, such as copious wavy shear bands and dimplelike patterns, are considered as strong evidence for the pronounced plastic deformation capability of ultrafine eutectic composites.

IV. SUMMARY

The partial substitution of iron by boron in $Fe_{87}Ti_7Zr_6$ ultrafine eutectic alloy induces significant changes of the microstructure and mechanical behavior, including strength and compressive plasticity. With increasing of the boron content to 6 at.%, the eutectic morphology becomes slightly modulated from regular lamellar to spherical cellular with spatial length-scale heterogeneity on the lamellar spacing and the mechanical properties are simultaneously improved. In particular, the $Fe_{83}Ti_7Zr_6B_4$ alloy shows interesting mechanical properties with an enhanced plasticity of 8% together with a high strength of 3.1 GPa. The improved plasticity is attributed to the rotational motion of spherical eutectic colonies with a distinct microstructural length-scale hierarchy of the lamellar spacing, resulting from a homogeneous distribution of the localized shear deformation throughout the entire sample. On the other hand, when more boron is added, multiphase composites containing a glassy phase form. They show a high strength of ~3.3 GPa but no plasticity. Therefore, the investigations reveal that the plasticity of Fe-based heterogeneous multiphase composites is decisively linked to the length scale variable and the crystallinity of the constituent phases.

ACKNOWLEDGMENTS

This work was supported by Defense Acquisition Program Administration (DAPA) and Agency for Defense Development (ADD), and also supported by the Global Research Laboratory Program of Korea Ministry of Science and Technology, and by the Center for Advanced Materials Processing (CAMP) of the 21st Century Frontier R&D Program of the Korea Ministry of Knowledge Economy. Stimulating discussions with A. Schlieter, E. Fleury, G. Wang, J.H. Han, M.H. Lee, O. Shuleshova, R. Li, S. Pauly, and W.T. Kim are gratefully acknowledged.

REFERENCES

1. M.C. Flemings: *Solidification Processing* (McGraw-Hill, New York, 1974).
2. M. Dao, L. Lu, R.J. Asaro, J.T.M. De Hosson, and E. Ma: Toward a quantitative understanding of mechanical behavior of nanocrystalline metals. *Acta Mater.* **55**, 4041 (2007).
3. C.A. Schuh, T.C. Hufnagel, and U. Ramamurty: Mechanical behavior of amorphous alloys. *Acta Mater.* **55**, 4067 (2007).
4. G. He, J. Eckert, W. Löser, and L. Schultz: Novel Ti-base nanostructure-dendrite composite with enhanced plasticity. *Nat. Mater.* **2**, 33 (2003).
5. J.M. Park, T.E. Kim, S.W. Sohn, D.H. Kim, K.B. Kim, W.T. Kim, and J. Eckert: High strength Ni–Zr binary ultrafine eutectic-dendrite composite with large plastic deformability. *Appl. Phys. Lett.* **93**, 031903 (2008).
6. J.W. Qiao, S. Wang, Y. Zhang, P.K. Liaw, and G.L. Chen: Large plasticity and tensile necking of Zr-based bulk metallic glass matrix composites synthesized by the bridgman solidification. *Appl. Phys. Lett.* **94**, 151905 (2009).
7. D.C. Hofmann, J.Y. Suh, A. Wiest, G. Duan, M.L. Lind, M.D. Demetrious, and W.L. Johnson: Designing bulk metallic glass matrix composites with high toughness and tensile ductility. *Nature* **451**, 1085 (2008).
8. S. Pauly, S. Gorantla, G. Wang, U. Kühn, and J. Eckert: Transformation-mediated ductility in CuZr-based bulk metallic glasses. *Nat. Mater.* **9**, 473 (2010).
9. D.V. Louzguine, H. Kato, L.V. Louzguina, and A. Inoue: High-strength binary Ti–Fe bulk alloys with enhanced ductility. *J. Mater. Res.* **19**, 3600 (2004).
10. L. Shi, H. Ma, T. Liu, J. Xu, and E. Ma: Microstructure and compressive properties of chill-cast Mg–Al–Ca alloys. *J. Mater. Res.* **21**, 613 (2006).
11. J.M. Park, N. Mattern, U. Kühn, J. Eckert, K.B. Kim, W.T. Kim, K. Chattopadhyay, and D.H. Kim: High strength bulk Al-based bimodal ultrafine eutectic composite with enhanced plasticity. *J. Mater. Res.* **24**, 2605 (2009).
12. H.K.D.H. Bhadeshia and R.W.K. Honeycombe: *Steel: Microstructure and Properties*, 3rd ed. (Butterworth-Heinemann Press, Oxford, UK, 2006).
13. B. Shen, H. Men, and A. Inoue: Fe-based bulk glassy alloy composite containing in situ formed α-(Fe, Co) and $(Fe, Co)_{23}B_6$ microcrystalline grains. *Appl. Phys. Lett.* **89**, 101915 (2006).
14. S.F. Guo, L. Liu, N. Li, and Y. Li: Fe-based bulk metallic glass matrix composite with large plasticity. *Scr. Mater.* **62**, 329 (2010).
15. K. Werniewicz, U. Kühn, N. Mattern, B. Bartusch, J. Eckert, J. Das, L. Schultz, and T. Kulik: New Fe–Cr–Mo–Ga–C composites with high compressive strength and large plasticity. *Acta Mater.* **55**, 3513 (2007).
16. R. Li, G. Liu, M. Stoica, and J. Eckert: FeCo-based multiphase composites with high strength and large plastic deformation. *Intermetallics* **18**, 134 (2010).
17. J.M. Park, S.W. Sohn, T.E. Kim, K.B. Kim, W.T. Kim, and D.H. Kim: Nanostructure-dendrite composites in the Fe–Zr binary alloy system exhibiting high strength and plasticity. *Scr. Mater.* **57**, 1153 (2007).
18. J.M. Park, K.B. Kim, M.H. Lee, W.T. Kim, J. Eckert, and D.H. Kim: High strength ultrafine eutectic Fe–Nb–Al composites with enhanced plasticity. *Intermetallics* **16**, 642 (2008).
19. M.L. Lee, Y. Li, and C.A. Schuh: Effect of controlled volume fraction of dendritic phases on tensile and compressive ductility in La-based metallic glass. *Acta Mater.* **52**, 4121 (2004).
20. D.C. Hofmann, J.Y. Suh, A. Wiest, M.L. Lind, M.D. Demetrious, and W.L. Johnson: Development of tough, low density titanium-based bulk metallic glass matrix composites with tensile ductility. *Proc. Natl. Acad. Sci. U.S.A.* **105**, 20136 (2008).
21. J.M. Park, S.W. Sohn, D.H. Kim, K.B. Kim, W.T. Kim, and J. Eckert: Propagation of shear bands and accommodation of shear strain in the $Fe_{56}Nb_4Al_{40}$ ultrafine eutectic-dendrite composite. *Appl. Phys. Lett.* **92**, 091910 (2008).
22. D.V. Louzguine, H. Kato, and A. Inoue: High-strength hypereutectic Ti–Fe–Co bulk alloy with good ductility. *Philos. Mag. Lett.* **84**, 359 (2004).

https://doi.org/10.1557/jmr.2010.50 Published online by Cambridge University Press

23. C. Fan, R.T. Ott, and T.C. Hufnagel: Metallic glass matrix composite with precipitated ductile reinforcement. *Appl. Phys. Lett.* **81**, 1020 (2002).
24. J.M. Park, D.H. Kim, K.B. Kim, E. Fleury, M.H. Lee, W.T. Kim, and J. Eckert: Enhancement of plasticity in Ti-rich Ti–Zr–Be–Cu–Ni–Ta bulk glassy alloy via introducing the structural inhomogeneity. *J. Mater. Res.* **23**, 2984 (2008).
25. H. Ma, L.L. Shi, J. Xu, and E. Ma: Chill-cast in situ composites in the pseudo-ternary Mg–(Cu, Ni)–Y glass-forming system: Microstructure and compressive properties. *J. Mater. Res.* **22**, 314 (2007).
26. C.C. Hay, C.P. Kim, and W.L. Johnson: Microstructure controlled shear band formation and enhanced plasticity of bulk metallic glasses. *Phys. Rev. Lett.* **84**, 2901 (2000).
27. J.M. Park: Mechanical behavior of bulk nano-/ultrafine structured composites. Ph.D. thesis, Yonsei University, Seoul, Korea, 2008.
28. JCPDFWIN: Version 2.2 (JCPDS, International Center for Diffraction Data, Newton Square, PA, 2001).
29. H. Okamoto: *Phase Diagrams for Binary Alloys* (ASM International, Materials Park, OH, 2000).
30. J.M. Park, D.H. Kim, K.B. Kim, and W.T. Kim: Deformation-induced rotational eutectic colonies containing length-scale heterogeneity in an ultrafine eutectic $Fe_{83}Ti_7Zr_6B_4$ alloy. *Appl. Phys. Lett.* **91**, 131907 (2007).
31. T.H. Courtney: *Mechanical Behavior of Materials* (McGraw-Hill, Boston, MA, 1998).
32. J.H. Han, K.B. Kim, S. Yi, J.M. Park, D.H. Kim, S. Pauly, and J. Eckert: Influence of a bimodal eutectic structure on the plasticity of a $(Ti_{70.5}Fe_{29.5})_{91}Sn_9$ ultrafine composite. *Appl. Phys. Lett.* **93**, 201906 (2008).
33. D.V. Louzguine, L.V. Louzguina, H. Kato, and A. Inoue: Investigation of Ti–Fe–Co bulk alloys with high strength and enhanced ductility. *Acta Mater.* **53**, 2009 (2005).
34. L. Fu, J. Yang, Q. Bi, and W. Liu: Enhanced ductility of dendrite-ultrafine eutectic composite Fe_3B alloy prepared by self propagating high temperature synthesis. *Adv. Eng. Mater.* **11**, 194 (2009).

https://doi.org/10.1557/jmr.2010.50 Published online by Cambridge University Press